Low-dose antibiotics can collapse gut bacterial populations via a gelation transition

Brandon H. Schlomann[1,2,*], Travis J. Wiles[1,*], Elena S. Wall[1], Karen Guillemin[1,3], Raghuveer Parthasarathy[1,2]

[1]Institute of Molecular Biology, University of Oregon, Eugene, Oregon, United States of America

[2]Department of Physics and Materials Science Institute, University of Oregon, Eugene, Oregon, United States of America

[3]Humans and the Microbiome Program, CIFAR, Toronto, Ontario M5G 1Z8, Canada

*Equal contributors

Abstract

Antibiotics can profoundly alter the intestinal microbiome even at the sublethal concentrations often encountered through environmental contamination. The mechanisms by which low-dose antibiotics induce large yet highly variable changes in gut communities have remained elusive. We therefore investigated the impact of antibiotics on intestinal bacteria using larval zebrafish, whose experimental tractability enables high-resolution in vivo examination of response dynamics. Live imaging revealed that sublethal doses of the common antibiotic ciprofloxacin lead to severe drops in bacterial abundance, coincident with changes in spatial organization that increase susceptibility to intestinal expulsion. Strikingly, our data can be mapped onto a physical model of living gels that links bacterial aggregation and expulsion to nonequilibrium abundance dynamics, providing a framework for predicting the impact of antibiotics on the intestinal microbiome.

Introduction

Antibiotic drugs induce large, long-lasting, and disease-associated alterations in the composition of the intestinal microbiota [1, 2, 3]. Even at concentrations well below the minimum

inhibitory levels of many bacteria, antibiotics can lead to major and highly variable changes in the gut microbiome through mechanisms that remain mysterious [2, 3, 4]. Sublethal antibiotics can also significantly alter animal physiology, a well-known example being the intentional growth enhancement of livestock, possibly through pathways mediated by the microbiome [2]. Low concentrations of antibiotics are often present in the environment as byproducts of unchecked agricultural and biomedical use, generating public health concerns associated with the emergence of drug resistance [5] as well as more direct impacts on human health [6]. It is therefore crucial to uncover the mechanisms by which sublethal antibiotics can reshape gut microbial communities. Understanding which particular bacterial strains are resilient or susceptible to antibiotic perturbations will allow us to predict the consequences of environmental contamination and harness antibiotics as a therapeutic tool for reshaping gut communities.

In vitro studies have shown that low-dose antibiotics can induce major morphological and behavioral changes in bacteria. In particular, they can promote a transition to a more aggregated growth mode marked by reduced flagellar motility, reduced division rates, and increased formation of adherent biofilms [5]. We therefore hypothesized that changes in the physical structure of intestinal bacterial populations play a major role in determining antibiotic response dynamics. This notion is supported by our previous work showing that natural bacterial aggregates are highly susceptible to intestinal transport driven by the propulsive forces within the vertebrate gut. For example, imaging-based studies in larval zebrafish have revealed that human-derived *Vibrio cholerae* can use its Type VI Secretion System to enhance intestinal contractions and dispel aggregated resident bacteria [7]; that disruption of transport by perturbation of the enteric nervous system can neutralize inter-bacterial competition [8]; and that the magnitude of a species self-cohesion is a strong predictor of its spatial distribution [9]. Work in mammalian hosts has also uncovered links between bacterial population architecture and persistence within the intestine; for example, antibody-mediated enchaining of *Salmonella* cells leads to increased clearance from the mouse intestine [10].

To investigate the potential of low-dose antibiotics to perturb the physical structure and persistence of bacterial populations, we performed live, three-dimensional imaging of the entire intestinal volume of larval zebrafish hosts (Fig 1A, 1B) at spatial and temporal resolutions not attainable in humans or other model vertebrates. We assessed response dynamics of individual bacterial populations after treatment with the antibiotic ciprofloxacin. Ciprofloxacin is widely used therapeutically and is often detected in environmental samples at ng/mL concentrations that are sublethal but capable of perturbing bacterial physiology [11]. We focused our study on two native zebrafish bacterial isolates that we previously characterized as representing the extremes of cohesion phenotypes [9]: *Vibrio cholerae* ZWU0020, hereafter referred to as *Vibrio*, which exists in the larval zebrafish intestine primarily as dense populations of highly motile and planktonic individuals (Fig 1C, Supplemental Movie 1), and *Enterobacter cloacae* ZOR0014, hereafter referred to as *Enterobacter*, which primarily forms large, dense bacterial aggregates with small sub-populations of non-motile planktonic cells (Fig 1D, Supplemental Movie 2) [12]. To delineate and quantify antibiotic responses without the complications of inter-bacterial competition, we studied *Vibrio* and *Enterobacter* separately in hosts that were initially raised germ-free (Methods).

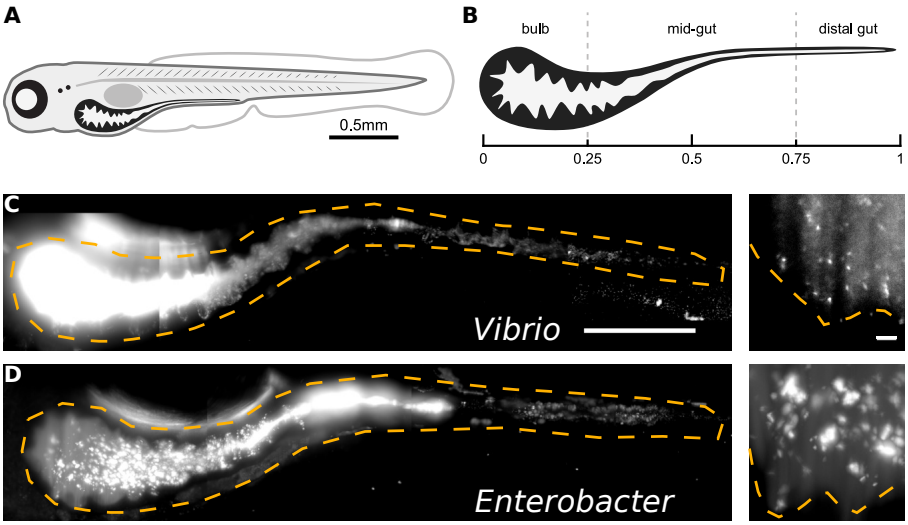

Figure 1: **Two bacterial species show different extremes of *in vivo* aggregation phenotypes.** A: Schematic of a 5 day-old zebrafish. B: Schematic of the larval zebrafish intestine. C: *Vibrio cholerae* ZWU0020 in vivo. Left: a maximum intensity projection of a three-dimensional image of the full gut. Dense, bright bacteria and dimmer intestinal autofluorescence are evident. The orange dashed curve indicates the approximate basal surface of the epithelium. Scale bar: 200 um. Right: a single optical plane within the anterior bulb in a fish colonized with 1:100 GFP:RFP-expressing *Vibrio*, with the GFP channel shown to highlight individual microbes in the dense swarm. The orange dashed curve indicates the approximate apical surface of the epithelium. Scale bar: 25 μm. (See also Supplemental Movie 1) D: *Enterobacter clocae* ZOR0014 in vivo, shown as a maximum intensity projection of the full gut (left) and a subset of the same projection in the anterior bulb (right); bacterial aggregates are evident.

As detailed below, we discovered that sublethal levels of ciprofloxacin lead to major reductions in intestinal abundance of both bacteria that cannot be predicted from in vitro responses, and that for both *Vibrio* and *Enterobacter* are linked to increased aggregation. Our findings highlight the delicate balance between individual cell growth and population cohesion that is necessary for stable residence, and show that antibiotics can shift this balance towards an unsustainable state that favors collapse and extinction. Surprisingly, quantitative image-derived population data motivate and are well fit by physical models originally used to describe colloidal growth and polymer gelation, implying an antibiotic-induced phase transition in bacterial community structure and revealing a general framework for understanding intestinal antibiotic perturbations.

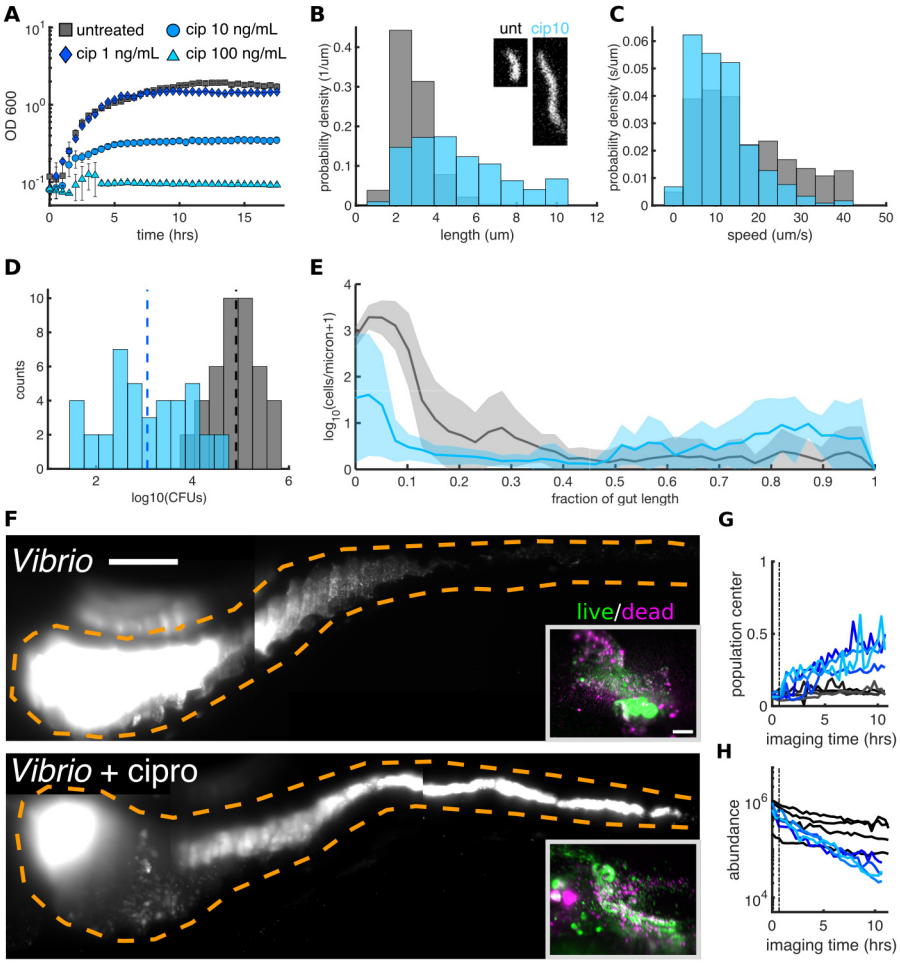

Figure 2: **Low-dose ciprofloxacin induces *Vibrio* aggregation and expulsion in vivo.** A: In vitro growth curves of *Vibrio* in rich media with different ciprofloxacin concentrations. B-E: In vitro and in vivo bacterial characteristics, with grey indicating experiments without antibiotic treatment and blue indicating exposure to 10 ng/mL ciprofloxacin. B: Distribution of *Vibrio* cell lengths. Insets show representative fluorescence microscopy images of untreated (left) and 10 ng/mL ciprofloxacin-treated (right) cells; inset widths = 3.5 μm. C: Distribution of in vitro swimming speeds of individual bacteria. D: Distributions of bacterial intestinal abundance of *Vibrio* mono-associated with larval zebrafish, assessed as colony forming units (CFUs) from plating of dissected gut contents. Counts indicate the number of individual fish with a given $\log_{10}$ *Vibrio* CFUs. Dashed lines indicate the mean of each set, showing a ∼100-fold reduction in intestinal *Vibrio* abundance in antibiotic-treated fish. E: Ensemble-averaged spatial distributions of log-transformed cell density as a function of distance along the gut axis, integrated over the perpendicular dimensions. F: Maximum intensity projections of 3D images of untreated (top) and ciprofloxacin-treated (bottom) *Vibrio* populations. Scale bar = 200 μm. Insets: Viability staining of bacteria expelled from the gut, with green and magenta indicating living and dead cells, respectively. Scale bar = 25 μm. G-H: Dynamics of in vivo *Vibrio* populations untreated (grey lines) and treated with 10 ng/mL ciprofloxacin (blue lines). G: 1D center of mass, normalized to intestine length. H: Total image-derived *Vibrio* abundance. In both (G) and (H), each curve represents a different zebrafish. Vertical dotted lines indicate the time of drug administration to the treatment cohort.

Low-dose cipro exposure increases aggregation and intestinal clearance

For both *Vibrio* and *Enterobacter*, we empirically determined a ciprofloxacin dosage that induced clear changes in bacterial physiology and behavior but that was below the apparent minimum inhibitory concentration for growth in rich media. We first describe results of antibiotic exposure, in vitro and in vivo, for the highly motile *Vibrio* species.

In vitro, the growth of *Vibrio* in lysogeny broth in the presence of 1 ng/mL ciprofloxacin closely resembles that of the untreated control, while a concentration of 100 ng/mL is largely inhibitory (Fig 2A). An intermediate concentration of 10 ng/mL leads to initially exponential growth at a rate (0.73 ± 0.08 hr^{-1}) indistinguishable from that of the untreated control (0.68 ± 0.07 hr^{-1}) (Methods), but a stationary phase density that is ∼5-fold lower than the untreated control. Viability staining (Methods) after 6 hours of incubation with 10 ng/mL ciprofloxacin (Supplemental Figure 1A and 1B) shows that the majority of the *Vibrio* population is alive. Growth in the presence of 10 ng/ml ciprofloxacin induces clear changes in cell morphology and motility: treated cells exhibit filamentation (Fig 2B), making them considerably longer (mean ± std. dev. 5.3 ± 3.1 um, n=963) than untreated *Vibrio* (2.9 ± 0.9 μm, n=2291) (Fig 2C). Swimming speed was also reduced compared to untreated cells (mean ± std. dev. 11.4 ± 7.2 μm/s, n=531, untreated (16.9 ± 11.1 μm/s, N=833) (Fig 2C, Supplemental Movies 3 and 4).

We then examined the effect of low-dose ciprofloxacin treatment on in vivo *Vibrio* populations. *Vibrio* was associated with germ-free zebrafish at 4 days post fertilization (dpf) by inoculation of the aqueous environment (Methods) and allowed to colonize for 24 hours, which from previous studies is known to provide ample time for the bacterial population to reach its carrying capacity [8]. Animals were treated by immersion in 10 ng/mL ciprofloxacin for 24 or 48 hours, or left untreated (Supplemental Figure 1E). *Vibrio* abundances were first assayed by gut dissection and plating to obtain measurements of colony forming units (CFUs) (Methods). Based on our in vitro characterizations, we expected a 1-10x decrease in *Vibrio* abundance. Surprisingly, we found a ∼100x reduction in mean abundance (Fig 2F). Pooled data from 24 and 48 hour treatments gives a mean ± std. dev. of the $\log_{10}$-transformed *Vibrio* population of 3.1 ± 0.9 (n=40), compared to 4.9 ± 0.5 (n=42) for untreated specimens (Fig 2F). Unpooled data are similar (Supplemental Figure 1F). This large reduction in *Vibrio* abundance suggests that the intestinal environment acts to amplify the severity of the ciprofloxacin treatment.

We assessed the possibility that the intestine makes *Vibrio* more susceptible to ciprofloxacin-induced cell death by embedding larval zebrafish in a weak agar gel, allowing collection of expelled bacteria. After staining with the viability dyes SYTO9 and propidium iodide (Methods) we imaged ejected material using light sheet fluorescence microscopy. We found no detectable difference between ciprofloxacin-treated and untreated populations (Fig 2F, insets), with both having a viable fraction of ∼50%, consistent with previous estimates of bacterial viability in the fecal material of healthy human adults in the absence of antibi-

otics [13]. This result suggests that the in vivo antibiotic-induced population decline is a consequence of the response of living bacteria to the intestinal environment.

We therefore used light sheet fluorescence microscopy (Methods) to directly observe and follow *Vibrio* populations in the intestines of live larval zebrafish over approximately 10 hours as they responded to antibiotic exposure. Three-dimensional time-lapse imaging revealed that upon ciprofloxacin treatment, large numbers of bacteria were depleted from the anterior-localized motile population, appearing instead in the mid- and distal regions of the gut, where they would further condense into multicellular aggregates or be expelled from the gut altogether (Supplemental Movie 5). After 10 hours of exposure, *Vibrio* populations in ciprofloxacin-treated hosts contained large, 3D aggregates localized to the posterior of the intestine, a feature not observed in untreated controls (Fig 2E,F) nor in all previous characterizations of this strain [8, 9].

Ciprofloxacin's mechanism of action involves inhibiting DNA replication, which often induces the coordinated expression of genes involved in DNA damage repair referred to as the SOS response [5]. We constructed a fluorescent reporter of the SOS response based on the DNA damage-inducible gene *recN* (Methods), and found that treatment of exponential phase *Vibrio* cells in vitro with 10 ng/mL ciprofloxacin induced the SOS response in ∼30% of cells (Supplemental Figure 1C,D). Further live imaging in vivo revealed that in ciprofloxacin-treated fish, SOS-positive cells exhibited more severe filamentation and reduced motility compared to SOS-negative cells within the same host (Supplemental Movie 6). In total, these processes of stress, filamentation, and aggregation result in the net posterior-directed movement of the center of mass of the bacterial population along the intestinal axis (Fig 2G, n=4 per case), culminating in expulsion from the host and a steep decline in total bacterial abundance (Fig 2H).

Low-dose cipro exposure can suppress small cluster reservoirs

In contrast to *Vibrio*, *Enterobacter* naturally forms dense aggregates in the zebrafish intestine. It would therefore be reasonable to expect *Enterobacter* populations to be more resistant to ciprofloxacin. However, as detailed below, we found this to be incorrect; *Enterobacter* exhibits even greater susceptibility to ciprofloxacin-mediated expulsion.

We first established in vitro that 25 ng/ml ciprofloxacin produces similar effects on *Enterobacter* growth as did 10 ng/mL exposure on *Vibrio* (Fig 3A). Ciprofloxacin-treated *Enterobacter* showed a mildly reduced growth rate (mean ± std. dev of 1.1± 0.1 hr^{-1}) compared untreated bacteria (1.6 ± 0.1 hr^{-1}), but with a ∼5x lower optical density during stationary phase. Viability staining showed an even lesser degree of cell death and damage as compared to *Vibrio*, with a viable fraction of ∼95% (Supplemental Figure A,B) and no difference in the viable fractions of bacteria expelled from the intestines of untreated and treated hosts

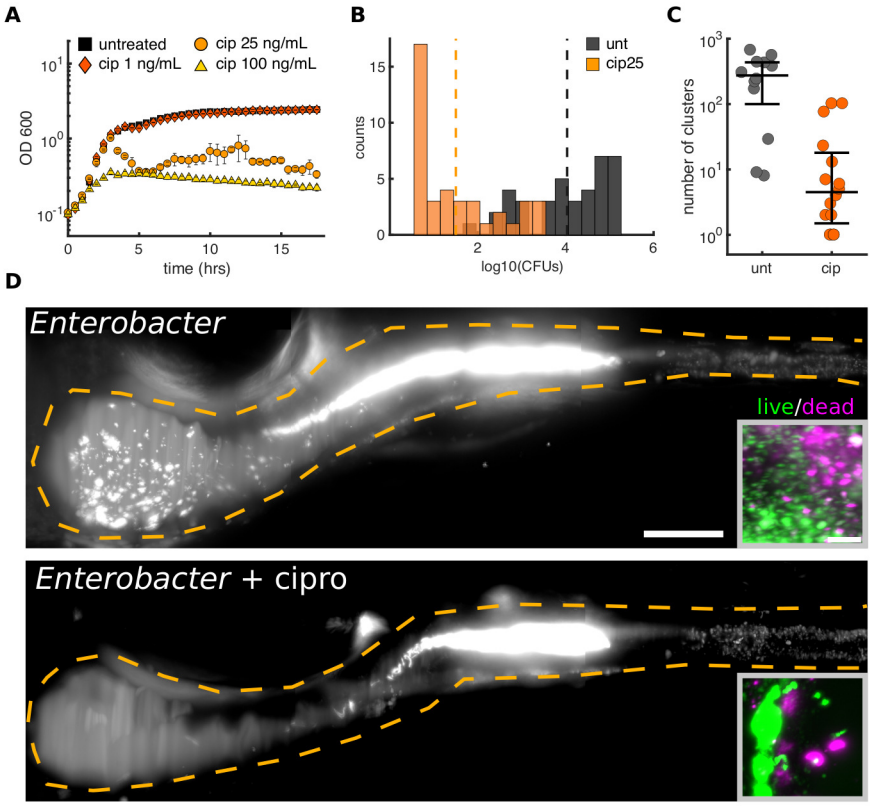

Figure 3: **Low-dose ciprofloxacin collapses *Enterobacter* populations and suppresses small clusters in vivo.** A: In vitro growth curves of *Enterobacter* in rich media with different ciprofloxacin concentrations. B-C: In vitro bacterial characteristics, with grey indicating experiments without antibiotic treatment and blue indicating 6 hours of exposure to 25 ng/mL ciprofloxacin. B: Distributions of bacterial intestinal abundance of *Enterobacter* mono-associated with larval zebrafish, assessed as colony forming units (CFUs) from plating of dissected gut contents. Counts indicate the number of individual fish with a given $\log_{10}$ *Enterobacter* CFUs. Dashed lines indicate the mean of each set, showing a ∼1000-fold reduction in intestinal *Enterobacter* abundance in antibiotic-treated fish. C: Total number of bacterial clusters in the intestine, with single cells defined as a cluster of size one, quantified from 3D images (Methods). D: Maximum intensity projections of 3D images of untreated (top) and ciprofloxacin-treated (bottom) *Enterobacter* populations. Scale bar = 200 μm. Insets: Viability staining of bacteria expelled from the gut, with green and magenta indicating living and dead cells, respectively. Scale bar = 10μm.

(Fig 3B). As with *Vibrio*, growth curves and viability assays both imply antibiotic-induced growth arrest rather than lethality at this ciprofloxacin concentration.

Strikingly, low-dose ciprofloxacin treatment of fish colonized with *Enterobacter* (Methods) resulted in even greater reductions in abundance than in the case of *Vibrio*, with the majority of populations becoming nearly or completely extinct during the assay period (Fig 3C). Inoculation, treatment, dissection, and plating were performed as for *Vibrio* (Methods). Pooled data from 24 and 48 hour treatments gives a mean $\pm$ std. dev. of the $\log_{10}$-transformed *Enterobacter* population of 1.5 ± 1.0 (n=40), compared to 4.0 ± 1.0 (n=39), for untreated specimens (Fig 3C); unpooled data are similar (Supplemental Figure 2C,D).

Live imaging of intestinal populations at single time points revealed approximately 40% of hosts to be devoid or nearly devoid of *Enterobacter*, consistent with the plating-based measurements. In the hosts that contained appreciable bacterial populations we observed a clear difference between treated and untreated specimens: *Enterobacter* populations in ciprofloxacin-treated hosts contained fewer small bacterial clusters and fewer individual planktonic cells than untreated controls (Fig 3E). We quantified this distinction using computational image analysis to identify each cluster (Methods), defining a single cell as a cluster of size one. Bacterial populations in ciprofloxacin-treated animals contained $\sim$80x fewer clusters than untreated animals (Fig 3F, top).

It is clear from previous studies of a variety of aggregated bacterial species that large clusters are susceptible to expulsion from the gut, driven by intestinal contractions [8, 7]. To establish whether this is also the case for *Enterobacter*, we performed time-lapse 3D imaging of untreated fish (Methods). Indeed, in 2 out of 5 hosts imaged for 3.5 hours each, we observed events in which the largest bacterial aggregate was abruptly expelled from the intestine (Fig 4A and Supplemental Movie 7). These time-lapse movies also showed clear examples of cluster aggregation (Supplemental Movie 8), in which bacterial clusters appear to come together and fuse, likely due to the rhythmic intestinal contractions that occur between frames. Importantly, smaller aggregates and planktonic cells, preferentially localized to the intestinal bulb, are relatively undisturbed during these dispersal events, save for a few clusters that become incorporated into the large mass during its transit (Supplemental Movie 7).

Our observations suggest a resolution to two related puzzles: how low-dose ciprofloxacin can lead to dramatic drops in *Enterobacter* abundance and, more generally, how naturally aggregating bacterial species can persist in the vertebrate gut despite the connection between aggregation and transport-driven expulsion. We provide both a qualitative and a quantitative description of the relevant dynamics, beginning with the following conceptual model: single cells of *Enterobacter* replicate to form small clusters, which then aggregate to form larger clusters under the influence of intestinal flow. Large clusters are transported by the rhythmic contractions of the gut [8, 7, 14] and stochastically expelled from the host [8, 7]. The individual bacteria and small clusters that remain within the intestine serve as a reservoir that reseeds the next population, and the process of replication, aggregation, and expulsion repeats. Therefore, persistence within the intestine requires processes that generate single cells or small clusters, otherwise transport will eventually lead to extinction. This

seeding could take the form of (i) immigration of new cells from the environment, (ii) passive fragmentation of clusters, or (iii) active fragmentation in which single cells break away from a cluster surface during cell division. Immigration from the environment likely occurs even in established populations, but measurements in larval zebrafish suggest very low rates [15]. We therefore we suspected that more robust mechanisms must promote persistence. Supporting the active fragmentation mechanism, we found in untreated hosts examples of populations that contain an abundance of single cells, a single large cluster, and a lack of mid-sized clusters (Supplemental Figure 2E). Following low-dose ciprofloxacin treatment, the planktonic cell reservoir required for resilience to intestinal transport is depleted (Fig 3C), most likely due to stalled *Enterobacter* division (Fig 3A), leading to collapse of the bacterial population (Fig 3B).

A quantitative model of bacterial cluster dynamics

To solidify and test our conceptual picture, we developed and validated a predictive mathematical model of bacterial cluster dynamics. Drawing on ideas from non-equilibrium statistical mechanics and soft matter physics, we constructed a general kinetic model that describes the time evolution of a collection of bacterial clusters with varying sizes, illustrated schematically in Fig 4B. We posit that four processes govern cluster dynamics: aggregation, fragmentation, growth, and ejection. Each is described by a kernel that specifies its rate and size dependence: (1) aggregation of a cluster of size n and a cluster of size m occurs with rate A_{nm}; (2) fragmentation of a cluster of size $n+m$ into clusters of size n and m occurs with rate F_{nm}; (3) growth (due to cell division) of a cluster of size n occurs with rate G_n; (4) expulsion (removal by intestinal transport) of a cluster of size n occurs with rate E_n. Note that condensation of the population into a single massive cluster poises the system for extinction, as long as E_n is nonzero. The model is non-spatial and is inspired by well established frameworks for nucleation and growth phenomena such as polymer gelation and colloidal aggregation [16]. For example, sol-gel models describe a transition between dispersed individual units ("sol") and a system-spanning connected network ("gel") in materials capable of polymerization. In the thermodynamic limit of infinite system size, the model can be studied using standard analytic techniques [16]. However, unlike polymer solutions and other bulk systems for which the possible number of clusters is effectively unbounded, our intestinal populations are constrained to have at most a few hundred clusters (Fig 3C), necessitating the use of stochastic simulations (Methods).

In its general form, the model encompasses a wide range of behaviors that can be encoded in the various functional forms possible for the rate kernels A_{nm} F_{nm}, G_n, and E_n. Our goal was to develop a framework that quantitatively predicts features of the *Enterobacter* cluster size distribution not explicitly encoded in the model, compare these to data, and following this validation gain general insights into perturbations and population stability. Based on our observations and theoretical considerations elaborated in the Methods section, we made the following assumptions: (1) the rate of aggregation between two clusters is independent of

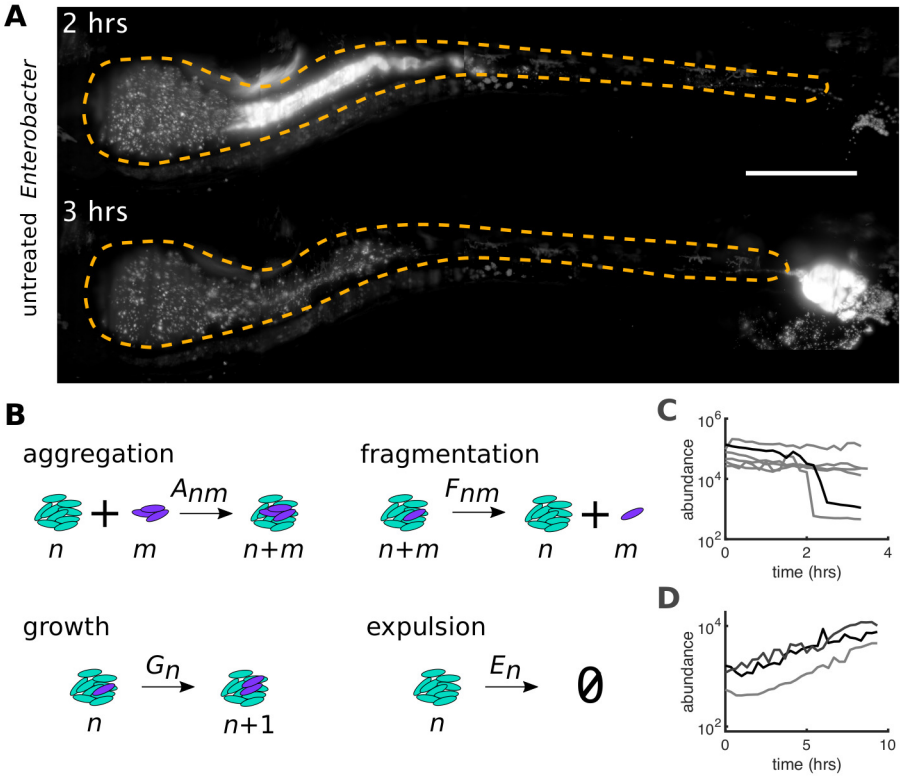

Figure 4: **Small bacterial clusters are required for recovery after large expulsion events.** A: Maximum intensity projections of untreated *Enterobacter* populations before (top, $t = 2$ hours from the start of imaging) and after (bottom, $t = 3$ hours) an expulsion event (See also Supplemental Movie 5). Scale bar = 200 μm. B: Schematic of a kinetic model of bacterial cluster dynamics, illustrating its four constituent processes. C: Image-derived time-series of *Enterobacter* abundance in five untreated hosts showing sporadic large expulsion events. The black line is from bacteria in the fish shown in (A). D: Image-derived quantification of initial population dynamics in three hosts showing in vivo *Enterobacter* growth.

their size, $A_{nm} = \alpha$; (2) fragmentation occurs only by separation of single cells and with a rate that is independent of cluster size, $F_{nm} = \beta$ for $m = 1$ and $F_{nm} = 0$ otherwise; (3) growth is logistic with a global carrying capacity, $G_n = rn(1 - N/K)$ with N the total number of cells, r the per capita growth rate, and K, the carrying capacity; (4) expulsion is independent of cluster size, $E_n = \lambda$. As discussed in the Methods section, these choices constitute the minimal model consistent with theoretical constraints and experimental phenomenology. More complex models are of course possible, but the requisite increase in the number of adjustable parameters would result in a trivial but meaningless ability to fit the observed data.

Even with the assumptions described above, the model needs 5 parameters: rates of aggregation, fragmentation, growth, and dispersal, and a global carrying capacity. However, all of these parameters can be set by experimentally derived values unrelated to cluster size distributions. We measured *Enterobacter*s per capita growth rate by performing time-lapse imaging of initially germ-free hosts that had been exposed to *Enterobacter* for only 8 hours, capturing the exponential increase of a small founding population (Fig 3D, Supplemental Movie 9), yielding $r = 0.27 \pm 0.05$ hr^{-1} (mean $\pm$ std. dev across $n = 3$ hosts). We identified expulsion events as abrupt collapses in *Enterobacter* abundance from time-lapse images (Fig. 3C, Supplemental Movie 7) and set the ejection rate equal to the measured collapse rate, $\lambda = 0.11 \pm 0.08$ hr^{-1} (mean $\pm$ standard error, assuming an underlying Poisson process (Methods)). The model can be simulated to provide the mean and variance of the $\log_{10}$-transformed abundance distribution at a given time for a given set of parameters. Using this, we fit static bacterial abundance measurements from dissection and plating at 72 hours post-inoculation (Methods) to determine the carrying capacity, K, and the ratio of fragmentation and aggregation rates, β/α. As discussed in the Methods section, the cluster dynamics should depend primarily on the ratio of β/α rather than either rate separately. This yielded $\log_{10} K = 5.0 \pm 0.5$ and $\log_{10} \beta/\alpha = 2.5 \pm 0.4$.

The parameter-free prediction of the size distribution of *Enterobacter* aggregates is plotted in Fig. 5A, together with the measured distribution derived from three-dimensional images from 12 untreated hosts; the two are in remarkable agreement. We also plot, equivalently, the cumulative distribution function $P(\text{size} > n)$, the probability that a cluster will contain greater than n cells, again illustrating the close correspondence between the data and the prediction and validating the model. We emphasize that no information about the cluster size distribution was used to estimate any of the model parameters.

The abundance phase diagram and extinction transition

Our kinetic model provides insights into the consequences of low-dose antibiotic perturbations on gut bacterial populations. We consider a general phase diagram of possible growth, fragmentation, aggregation, and expulsion rates, and then situate *Enterobacter* in this space. For simplicity of illustration, we consider a two-dimensional representation with one axis being the ratio of the fragmentation and aggregation rates, β/α, and the other being the ratio

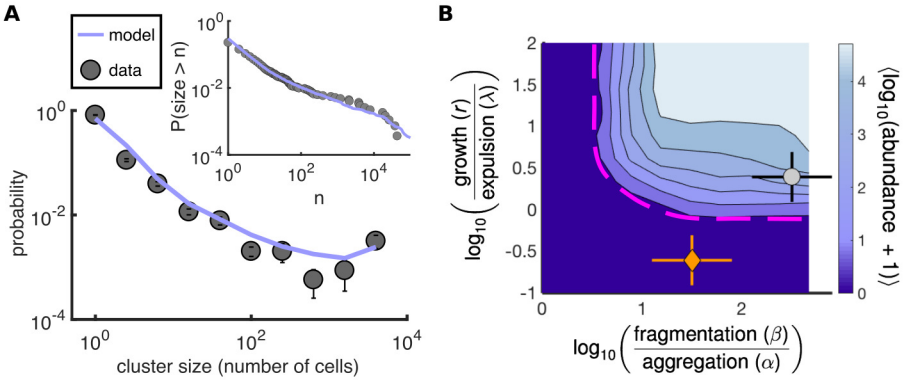

Figure 5: **A stochastic kinetic model predicts bacterial cluster sizes and generates a phase diagram for in vivo abundance.** A: The distribution of image-derived *Enterobacter* cluster sizes (grey circles) along with the parameter-free prediction of our stochastic model (purple line). Parameters: $r = 0.27$ hr^{-1}, $\lambda = 0.11$ hr^{-1}, $\alpha = 0.1$ hr^{-1}, $\beta = 10^{1.5}$ hr^{-1}, $K = 10^5$. Error bars are standard deviations across resampled datasets. Inset: The same data and model plotted without binning as a reverse cumulative distribution. B: Phase diagram of the log-transformed abundance, $\langle \log_{10}(N+1) \rangle$, showing the extinction transition (magenta dashed line). From best fit parameter estimates, the in vivo states of untreated *Enterobacter* is overlaid as white circle, and 25 ng/ml ciprofloxacin-treated *Enterobacter* as an orange diamond. Parameters: $\lambda = 0.11$ hr^{-1}, $\alpha = 0.1$ hr^{-1}, $K = 10^5$ were fixed; r and β were varied on a logarithmic grid.

of the growth and expulsion rates, r/λ (Fig 5B). As noted above and in the Methods section, the model in the regime studied should depend on the ratio β/α rather than on β or α independently. However, the roles of r and λ are not simply captured by their ratio. The expulsion rate nonetheless provides a scale to which to compare the growth rate, r, and we plot Fig 5B using r/λ calculated for fixed $\lambda = 0.11$ hr^{-1}, the measured value. For completeness, we show a three-dimensional $r, \lambda, \beta/\alpha$ phase diagram as Supplemental Figure 3E,F. We numerically calculated the steady state phase diagram of the model (Methods) and show in Figure 5B the mean log-transformed abundance, $\langle \log_{10}(N+1) \rangle$. The regime of extinction ($N = 0$) is evident (magenta curve).

The data-derived parameter values place untreated intestinal *Enterobacter* fairly close to the extinction transition (Fig. 5B). An antibiotic-induced growth rate reduction of ∼5x is sufficient to cross the boundary to the N=0 regime (i.e. to extinction), moving downward in Fig 5B. This growth rate reduction, or an equivalent increase in death rate, reflects the conventional view of antibiotic effects. A ∼300x reduction in the balance between fragmentation and aggregation spurs an alternative path to extinction, moving leftward in Fig 5B, reflecting a distinct mechanism resulting solely from changes in physical structure. The extinction transition in this direction corresponds to the condensation of the population into a single cluster, reminiscent of gelation phase transitions in polymer systems. As described above, low-dose ciprofloxacin causes a strong reduction in the number of small bacterial clusters, lowering β and possibly also r if fragmentation and individual cell division are linked. Conservatively assuming an equal effect along both axes, and fitting simulations to the 24 hour

treatment abundances (Methods), we find that the antibiotic reduces r and β/α by $\sim$10x. This drives the bacterial system through the phase boundary and well into the extinction regime (Fig 5B, orange diamond), consistent with our observations.

Conclusions

We have discovered that sublethal levels of a commonly used antibiotic can reduce the intestinal abundance of bacterial populations much more severely than would be predicted from in vitro responses, and that this amplification is a consequence of drug-induced changes to the spatial architecture of microbial communities. Live imaging revealed drug-induced increases in bacterial cohesion that, coupled to gut mechanical activity, lead to the expulsion of viable microbial cells. Notably, the underlying processes of bacterial motility and aggregation and host intestinal transport are found throughout the animal kingdom, suggesting a general relevance beyond zebrafish that may explain, for example, data on weak antibiotics having strong effects on mammalian microbiomes [2, 3]. Of course, chemical perturbations in more anatomically complex animals or non-gnotobiotic animals that house hundreds of resident bacterial species will undoubtedly involve additional processes beyond those uncovered here. We note, however, that responses to intestinal flow will influence bacterial population dynamics regardless of ecological complexity, and that our choice of model bacterial species spans the extremes of highly planktonic and highly cohesive strains, further implying generality. In the larval zebrafish, enhanced bacterial susceptibility to transport leads to expulsion from the gut. In larger or more complex intestines this may take the form of displacement from one region to a more distal region, with a corresponding shift in local nutrients or competitors, in addition to expulsion from the gut altogether.

The concentrations of ciprofloxacin examined here are commonly found in environmental samples, indicating a potentially widespread perturbation of animal gut microbiota due to antibiotic contaminants. In addition, the expulsion of live, antibiotic-exposed bacteria from animal intestines through the aggregation-based mechanisms described here suggests a previously unrecognized path for the spread of resistance mechanisms. Together, these observations amplify recent concerns about the public health risk posed by antibiotic contaminants in the environment [6].

Our biophysical model of cohesion, aggregation, growth, and expulsion not only describes our data and provides testable predictions, but also supplies a framework for a quantitative understanding of gut microbial homeostasis. It is remarkable, given the chemical and morphological complexity of even the larval zebrafish gut, that such a minimal model can predict emergent properties such as the size distribution of bacterial aggregates. That this works is an indication of the power of theories of soft condensed matter physics, whose relevance to the gut microbiome has never before been realized. Inter-species interactions in conventional intestinal microbiomes, conversely, point to further extensions of theory beyond those described here.

The main prediction of our model is that naturally aggregated, slow growing species will be impacted more severely than fast growing, planktonic species by equivalent low-dose antibiotic perturbations. Such species are situated closer to the extinction phase boundary (Fig 5B), beyond which stable nonzero populations are impossible to maintain. With continued advancements in histological sample preparation [17] and meta-omics analyses [18], it may soon be possible to gather data with which to test this prediction in less tractable host species, such as mice and humans. A further prediction is that intestinal transport, which has been linked to microbiota composition [19], will influence the effects of low-dose antibiotic perturbations on microbial community composition. Combining pharmacological manipulations of intestinal transport with antibiotic treatments may therefore lead to novel strategies for precision engineering of the gut microbiome.

Acknowledgements

Research was supported through the M.J. Murdock Charitable Trust and an award from the Kavli Microbiome Ideas Challenge, a project led by the American Society for Microbiology in partnership with the American Chemical Society and the American Physical Society and supported by The Kavli Foundation. Work was also supported by the National Science Foundation under Awards 1427957 and 0922951. Authors received funding from the National Institutes of Health (http://www.nih.gov/), P50GM09891 and P01GM125576-01 to K.G. and R.P., F32AI112094 to T.J.W., and T32GM007759 to B.H.S.

Methods

Animal care

All experiments with zebrafish were done in accordance with protocols approved by the University of Oregon Institutional Animal Care and Use Committee and following standard protocols [20].

Gnotobiology

Wild-type (AB×TU strain) zebrafish were derived germfree (GF) and colonized with bacterial strains as previously described [21] with slight modifications. Briefly, fertilized eggs from adult mating pairs were harvested and incubated in sterile embryo media (EM) containing ampicillin (100 μg/ml), gentamicin (10 μg/ml), amphotericin B (250 ng/ml), tetracycline (1 μg/ml), and chloramphenicol (1 μg/ml) for 6 h. Embryos were then washed in EM containing 0.1% polyvinylpyrrolidone-iodine followed by EM containing 0.003% sodium hypochlorite.

Sterilized embryos were distributed into T25 tissue culture flasks containing 15 ml sterile EM at a density of one embryo per milliliter and incubated at 28 to 30°C prior to bacterial colonization. Embryos were sustained on yolk-derived nutrients and were not fed during experiments. For bacterial mono-association, bacteria were first grown overnight in lysogeny broth (LB) with shaking at 30°C and were prepared for inoculation by pelleting 1 ml of culture for 2 min at 7,000×g and washing once in sterile EM. Bacterial strains were individually added to the water column of single flasks containing 4-day-old larval zebrafish at a final density of 10^6 bacteria/ml. For antibiotic treatment, drugs were added at the indicated working concentration directly to flask containing animals that had been colonized 24 h prior.

Bacterial strains and culture

Vibrio cholerae ZWU0020 and *Enterobacter cloacae* ZOR0014 were originally isolated from the zebrafish intestine [22]. Fluorescently marked derivatives of each strain were previously generated by Tn7-mediated insertion of a single, constitutively expressed gene encoding dTomato [12]. Vibrio cholerae ZWU0020 encoding a fluorescent DNA-damage (SOS) reporter was generated by fusing the promoter region of the *recN* gene (100 bp upstream of the start codon), which harbors three predicted LexA binding sites, to an open reading frame encoding superfolder green fluorescent protein (sfGFP). The resulting synthetic construct was inserted into a Tn7 delivery vector containing a constitutively expressed dTomato gene, which allows tracking of all bacterial cells. The resulting dual-reporter construct was then inserted into the ZWU0020 genome as previously described [12]. We note that all plating- and imaging-based experiments performed in this study were done using fluorescently marked strains, with the exception of experiments in which fluorescent dyes were used to assess viability of cells. Archived stocks of bacteria were maintained in 25% glycerol at ∼80°C. Prior to experiments, bacteria were directly inoculated from frozen stocks into 5 mL LB media (10 g/L NaCl, 5 g/L yeast extract, 12 g/L tryptone, 1 g/L glucose) and grown for 16 h (overnight) shaking at 30°C.

In vitro characterization of antibiotics

Growth kinetics: Growth kinetics of bacterial strains in vitro were measured using a FLUOstar Omega microplate reader. Prior to growth measurements, bacteria were grown overnight in 5 ml LB media at 30°C with shaking. The next day, cultures were diluted 1:100 into fresh LB media with or without the indicated antibiotic and dispensed in quadruplicate (200 μl/well) into a sterile 96-well clear flat-bottom tissue culture-treated microplate. Absorbance at 600 nm was then recorded every 30 min for ∼16 h at 30°C with shaking. Growth rates were estimated by fitting a logistic growth curve to OD values, starting at manually defined points marking the end of lag phase.

Viability: Cultures of *Vibrio* ZWU0020 or *Enterobacter* ZOR0014 were grown overnight in

LB at 30°C with shaking. The next day, 1:100 dilutions were made in fresh LB media containing either ciprofloxacin (*Vibrio*: 10 ng/ml, *Enterobacter*: 25 ng/ml) or no drug. Cultures were incubated at 30°C with shaking for 6 h prior to being stained using a LIVE/DEAD BacLight Bacterial Viability Kit according to manufacturers instructions. Culture/stain mixtures were diluted 1:10 in 0.7% saline and imaged using a Leica MZ10 F fluorescence stereomicroscope equipped with a 2.0X objective and Leica DFC365 FX camera. Images were captured using standard Leica Application Suite software. Bacteria were identified in images with intensity-based region finding following difference of gaussians filtering. Cells stained in both SYTO9 and propridium iodide were identified as overlapping regions in the two color channels. Analysis code was written in MATLAB.

Cell length and swimming speed: Dense overnight cultures of Vibrio ZWU0020 were diluted 1:100 in fresh LB media alone or with 10 ng/ml ciprofloxacin and incubated at 30°C with shaking for 4 h. Bacteria were then imaged on a Nikon TE2000 inverted fluorescence microscope between a slide and a coverslip using a 60X oil immersion objective and a Hamamatsu ORCA CCD camera (Hamamatsu City, Japan). Movies were taken within 60 seconds of mounting at an exposure time of 30 ms, resulting in a frame rate of 15 frames/sec. Bacteria in the resulting movies were identified with intensity-based region finding and tracked using nearest-neighbor linking. Analysis code was written in MATLAB.

Vibrio SOS reporter activity: Vibrio ZWU0020 carrying the fluorescent SOS reporter was grown overnight in LB at 30°C with shaking. The next day, 1:100 dilutions were made in fresh LB media containing either 10 ng/ml ciprofloxacin, 400 ng/ml mitomycin C, 10 μg/ml ampicillin, or no drug. Cultures were then grown overnight ($\sim$16 h) at 30°C with shaking. The next day, cultures were diluted 1:43 in 80% glycerol (as an immobilizing agent) and imaged with a Nikon Eclipse Ti inverted microscope equipped with an Andor iXon3 888 camera using a 40x objective and 1.5x zoom. Bacteria were identified in images with gradient-based region finding, using a Sobel filter, following difference of gaussians filtering. Analysis code was written in MATLAB. As expected, the two DNA targeting drugs, ciprofloxcain and mitomycin C, induced the SOS response in subpopulations of cells, while the cell-wall targeting drug ampicillin did not.

Culture-based quantification of bacterial populations

Dissection of larval guts was done as described previously [23]. Dissected guts were harvested and placed in a 1.6 ml tube containing 500 μl sterile 0.7% saline and $\sim$100 μl 0.5 mm zirconium oxide beads. Guts were then homogenized using a bullet blender tissue homogenizer for $\sim$25 seconds on power 4. Lysates were serially plated on tryptic soy agar (TSA) and incubated overnight at 30°C prior to enumeration of CFU and determination of bacterial load. Typically an overnight incubation is sufficient to recover all viable cells; however, we note that ciprofloxacin treatment results in delayed colony growth on agar plates (likely due to growth arrest induced by DNA-damage). We empirically determined that, in the case of ciprofloxacin treatment, an incubation period 72 h was required for complete resusetation of

viable cells on agar plates. For all culture-based quantification of bacterial populations in this study, the estimated limit of detection is 5 bacteria/gut and the limit of quantification is 100 bacteria/gut. Plating data plotted are pooled from a minimum of two independent experiments. Samples with zero countable colonies on the lowest dilution were set to the limit of detection prior to plotting and statistical analysis.

Light sheet fluorescence microscopy of live larval zebrafish

Imaging intestinal bacteria: Live imaging of larval zebrafish was performed using a custom-built light sheet fluorescence microscope previously described in detail [24]. Larvae are anesthetized with MS-222 (Tricane) and mounted into small glass capillaries containing 0.5% agarose gel by means of a metal plunger. Larvae are then suspended vertically into an imaging chamber filled with embryo media and anesthetic and extruded out of the capillary such that the set agar plug sits in front of the imaging objective. The full intestine volume ($\sim$1200 $\times$ 300 $\times$ 150 microns) is imaged in four subregions that are registered in software after imaging. The imaging of a full intestine volume sampled at 1-micron steps between z-planes is imaged in $\sim$45 seconds. Excitation lasers at 488 and 561 nm wavelengths were tuned to a power of 5 mW prior to entering the imaging chamber. A 30 ms exposure time was used for all 3D scans and 2D movies. Time lapse imaging was performed overnight, except for the 3.5 hour imaging of Enterobacter (Fig 3C), which occurred during the day.

Viability staining of expelled aggregates: Germ-free larval zebrafish were colonized with wild type *Vibrio* or *Enterobacter* (without fluorescent markers) for 24 hours and then mounted into agar plugs using small glass capillaries identically to the imaging procedure (above). Individual capillaries were suspended into isolated wells of a 24-well tissue culture plate filled with embryo media containing anesthetic or anesthetic + ciprofloxacin (10 ng/mL for *Vibrio*, 25 ng/mL for *Enterobacter*) and the larvae were extruded from the capillaries. Fish remained mounted for 24 hours, during which expelled bacteria remained caught in the agar plug. After treatment, fish were pulled back into the capillaries and transferred to smaller wells of a 96 well plate containing embryo media, anesthetic, and the LIVE/DEAD BacLight Bacterial Viability stains SYTO9 and propridium iodide. Fish were stained for 30 min, pulled again into the capillaries, and transferred to the light sheet microscope for imaging.

Image analysis

Bacteria were identified in three-dimensional light sheet fluorescence microscopy images using a custom MATLAB analysis pipeline previously described [24, 9], with minor changes. In brief, small objects (single cells and small aggregates) are identified using difference of gaussians filtering. False positives are rejected with a combination of intensity thresholding (mostly noise) and manual removal (mostly host cells). Large aggregates are identified with

a graph cut algorithm [25] that is seeded with either an intensity-based mask or a gradient-based mask. The average intensity of a single cell is estimated as the mean intensity of small objects, which is then used to estimate the number of cells contained in larger clusters by normalizing the total fluorescence intensity of each cluster. Spatial distributions along the length of the gut are computed using a manually drawn line drawn that defines the guts center axis.

Kinetic model and stochastic simulations

Choosing rate kernels: Our approach to choosing the size dependence of the rate parameters was to pick the simplest kernels consistent with key experimental observations. The first key observation, made from past work [24, 8], was that in between the expulsion of large aggregates population growth is well described by a deterministic logistic function. Therefore, we naturally chose a logistic growth kernel. The second key observation was that we occasionally encountered populations consisting of just a single, large aggregate and many single cells (Supplemental Figure 2E), which suggests that active fragmentation of single cells, most likely during growth phases, is the dominant fragmentation process. This notion is supported by a time-lapse movie of initial growth (Supplemental Movie () that depicts the creation of single cells during growth, in addition to the growth of three dimensional aggregates. Based on these observations, we made the assumption that single cell fragmentation is the sole fragmentation process, leading to what's known as a "chipping" kernel [16]. Beyond the chipping assumption, we had little evidence that informed how single cell fragmentation depends on the size of the aggregate, so we opted for the simplest choice of a constant, size-independent rate. Similarly for aggregation and expulsion, the size dependence of the rates is in reality determined by complicated fluid mechanical interactions of bacterial clusters in peristaltic-like flow. Rather than attempt to capture these interactions in the rate kernels, we chose the simple form of a constant kernel for both processes.

With these choices, the model can be summarized by a Smoluchowski equation, which describes the time evolution of the concentration of clusters of size n, c_n, in the thermodynamic limit of infinite system size:

$$\begin{aligned}\dot{c}_n = \; & \frac{\alpha}{2}\sum_{m=1}^{n} c_{n-m}c_m - \alpha c_n \sum_{m=1}^{\infty} c_m + \beta(c_{n+1} - c_n) + \beta\delta_{n,1}\sum_{m=1}^{\infty} c_m \\ & + r\left(1 - \frac{\sum_{m=1}^{\infty} m c_m}{K}\right)\left[(n-1)c_{n-1} - n c_n\right] - \lambda c_n. \end{aligned} \tag{1}$$

The four rate parameters are α (aggregation), β (fragmentation), r (growth), and λ (expulsion), and K is the carrying capacity. In the last term of the first line, $\delta_{n,1}$ is the Kronecker delta with second argument equal to 1. Of note, the first line of equation (1), containing just aggregation and fragmentation terms, was previously studied as a model of polymer chains

and was shown to exhibit interesting non-equilibrium steady states and scaling behaviors that are due to the breaking of detailed balance by the chipping kernel [26]. In our system detailed balance is also broken, but for a different reason: our "monomers"—single cells—are alive and self-replicating.

Simulations: As each zebrafish intestine contains at most a few hundred bacterial clusters, finite size effects and stochasticity impact cluster statistics, so we implemented the model as a hybrid deterministic-stochastic simulation that follows the time evolution of individual clusters. Gillespie's direct method [27] was used to simulate stochastic aggregation, fragmentation, and expulsion events. Growth was treated as deterministic. Once the time until next stochastic reaction, τ, was determined according to the Gillespie algorithm, integration was performed with the Euler method from time t to $t + \tau$ using a time step $\Delta t = \min(\tau, 0.1 \text{ hr})$. The simulation was written in MATLAB and code is available at `https://github.com/bschloma/gac`.

Parameter inference

The kinetic model presented in the main text has 5 parameters: rates of growth, expulsion, aggregation, and fragmentation, along with an overall carrying capacity. As discussed in the main text, we directly measured *Enterobacter*'s growth rate and expulsion rate through time-lapse imaging. The uncertainty of the expulsion rate was estimated by the standard error, using the previously validated assumption that the expulsion of large aggregates follows a Poisson process [8]:

$$\mathrm{SE}_\lambda = \frac{\sqrt{\text{mean number of expulsions}}}{(\text{imaging time}) \times \sqrt{\text{number of fish}}}. \tag{2}$$

For the remaining parameters, we developed a method to infer them from the distribution of abundances obtained from dissection and plating assays. In a regime where aggregation and fragmentation are fast compared to expulsion, we expect the system to locally reach a quasi-steady state in between expulsions of the largest aggregates. As such, we expect cluster statistics to depend primarily on the ratio of fragmentation to aggregation, β/α, rather than on each rate independently. This confirmed in simulations (Supplemental Figure 3A,B). Therefore, the number of parameters to be estimated is reduced to two: β/α and K.

Untreated Enterobacter: We fixed $\alpha = 0.1 \text{ hr}^{-1}$ and performed a grid search in β and K on a logarithmic grid, simulating the model multiple trials for each pair of (β, K). The number of trials decreased with increasing β, from 1000 to 10. Each simulation started from 10 single cells and ran for a simulated time of 64 hours, modeling our 72 hour colonization data with an 8 hour colonization window. To model host-host variation, we drew each carrying capacity from a log-normal distribution with a standard deviation of 0.5 decades, roughly the value for the *Vibrio* abundance distribution (Supplemental Figure 1F). We then compared

the mean (μ) and variance (σ) of the simulated, log-transformed abundances $\log_{10}(N+1)$ with the values for our plating data ($\hat{\mu}$ and $\hat{\sigma}$, respectively), quantifying error using

$$\chi^2 = (\mu - \hat{\mu})^2 + (\sigma - \hat{\sigma})^2. \tag{3}$$

A heat map of χ^2 shows well-defined edges for the minimum values of the fit parameters (Supplemental Fig 3C). However, the inference is poorly constrained for carrying capacities larger than 10^5 and for $\log_{10}\beta/\alpha$ greater than 2.5. This poor constraint is due primarily to the insensitivity of the abundance distribution to increasing values of these parameters. For example, moving to the far right side of the abundance phase diagram in Fig 5B, the contours become flat in β/α.

To further constrain our estimates, we place upper bounds on these parameters with simple estimates of physical limits. To bound the carrying capacity, we note that a larval zebrafish intestine have a volume of roughly 1 nL, or 10^6 μm^3. Taking the volume of a bacterium to be roughly 1 μm^3, we estimate a maximum bacterial load of 10^6 cells, consistent with the largest *Vibrio* abundances (Supplemental Figure 1F). As we find no *Enterobacter* populations above $10^{5.5}$, and in our simulations we draw carrying capacities from a log-normal distribution with a standard deviation of half a decade, we report a best fit estimate of $\log_{10} K = 5.0$. To bound the fragmentation rate, β, we considered the time-lapse movie that showcases the greatest degree of cluster fragmentation observed (Supplemental Movie 9). This movie depicts the initial growth phase, in which both the size of aggregates and the number of single cells increase. Because the aggregates visibly grow in size, we know that the fragmentation rate must be bounded by the absolute growth rate of the population, $\beta < rN$; if the fragmentation rate were larger, cells would break off of the aggregate faster than they would be produced by cell division, and the aggregates would shrink in size. Taking, roughly, $r \sim 10^{-1}$ and $N \sim 10^3$ (Fig 4D), we estimate that $\beta < 10^2$, or, with $\alpha = 10^{-1}$, $\beta/\alpha < 10^3$. With this bound, we report a best fit estimate of $\log_{10}\beta/\alpha = 2.5$. We took the uncertainties of the best fit estimates, $\sigma_{\log_{10} K}$ and $\sigma_{\log_{10}\beta/\alpha}$, to be the inverse of the local curvatures of χ^2 at the best fit values: $\sigma_\theta = 1/|\partial_\theta^2 \chi^2|$, for $\theta = \log_{10} K$, $\log_{10}\beta/\alpha$, resulting in $\sigma_{\log_{10} K} = 0.5$ and $\sigma_{\log_{10} K} = 0.4$.

Ciprofloxacin-treated Enterobacter: To estimate the change in *Enterobacter*'s parameters upon antibiotic treatment, we conservatively assumed equal effect on growth and fragmentation/aggregation and modeled treatment parameters as $r' = \epsilon r$ and $\beta' = \epsilon\beta$. We then performed a single parameter grid search of ϵ values, ranging from $10^{-1.75}$ to $10^{-0.5}$. We modeled the antibiotic treatment as a parameter quench with a 6 hour buffer time, in which the antibiotics entered the intestine and began to take action on the bacteria. The value of 6 hours was chosen based on the *Vibrio* time series data. Each simulation was initialized with a cluster configuration drawn randomly from the imaging-derived dataset of actual untreated *Enterobacter* populations. The parameters r, λ, and K were set to their best fit or measured values, α was again fixed at 0.1 hr^{-1}, and r and β were both scaled by the same factors of ϵ. We then ran simulations for a modified simulation time $24 - 6 = 18$ hours and fit the mean and standard deviation of shifted log-transformed abundances measured in the

24 hour treatment plating assays. A plot of χ^2 vs ϵ shows a clear minimum at $\epsilon = 10^{-1}$ (Supplemental Figure 3D).

References

[1] Les Dethlefsen and David A. Relman. Incomplete recovery and individualized responses of the human distal gut microbiota to repeated antibiotic perturbation. *Proceedings of the National Academy of Science*, 108, 2011.

[2] Ilseung Cho, Shingo Yamanishi, Laura Cox, Barbara A Methé, Jiri Zavadil, Kelvin Li, Zhan Gao, Douglas Mahana, Kartik Raju, Isabel Teitler, et al. Antibiotics in early life alter the murine colonic microbiome and adiposity. *Nature*, 488(7413):621, 2012.

[3] Anjelique F Schulfer, Jonas Schluter, Yilong Zhang, Quincy Brown, Wimal Pathmasiri, Susan McRitchie, Susan Sumner, Huilin Li, Joao B Xavier, and Martin J Blaser. The impact of early-life sub-therapeutic antibiotic treatment (stat) on excessive weight is robust despite transfer of intestinal microbes. *The ISME journal*, page 1, 2019.

[4] Christopher A Gaulke, Carrie L Barton, Sarah Proffitt, Robert L Tanguay, and Thomas J Sharpton. Triclosan exposure is associated with rapid restructuring of the microbiome in adult zebrafish. *PLoS One*, 11(5):e0154632, 2016.

[5] Dan I Andersson and Diarmaid Hughes. Microbiological effects of sublethal levels of antibiotics. *Nature Reviews Microbiology*, 12(7):465, 2014.

[6] Engineering "National Academies of Sciences, Medicine, and others". *Environmental Chemicals, the Human Microbiome, and Health Risk: A Research Strategy*. National Academies Press, 2018.

[7] Savannah L. Logan, Jacob Thomas, Jinyuan Yan, Ryan P. Baker, Drew S. Shields, Joao B. Xavier, Brian K. Hammer, and Raghuveer Parthasarathy. The Vibrio cholerae type VI secretion system can modulate host intestinal mechanics to displace gut bacterial symbionts. *Proceedings of the National Academy of Sciences*, 115(16):E3779–E3787, 2018.

[8] Travis J. Wiles, Matthew Jemielita, Ryan P. Baker, Brandon H. Schlomann, Savannah L. Logan, Julia Ganz, Ellie Melancon, Judith S. Eisen, Karen Guillemin, and Raghuveer Parthasarathy. Host Gut Motility Promotes Competitive Exclusion within a Model Intestinal Microbiota. *PLoS Biology*, 14(7):1–24, 2016.

[9] Brandon H Schlomann, Travis J Wiles, Elena S Wall, Karen Guillemin, and Raghuveer Parthasarathy. Bacterial cohesion predicts spatial distribution in the larval zebrafish intestine. *Biophysical journal*, 115(11):2271–2277, 2018.

[10] Kathrin Moor, Médéric Diard, Mikael E. Sellin, Boas Felmy, Sandra Y. Wotzka, Albulena Toska, Erik Bakkeren, Markus Arnoldini, Florence Bansept, Alma Dal Co, Tom Völler, Andrea Minola, Blanca Fernandez-Rodriguez, Gloria Agatic, Sonia Barbieri, Luca Piccoli, Costanza Casiraghi, Davide Corti, Antonio Lanzavecchia, Roland R. Regoes, Claude Loverdo, Roman Stocker, Douglas R. Brumley, Wolf Dietrich Hardt, and

Emma Slack. High-avidity IgA protects the intestine by enchaining growing bacteria. *Nature*, 544(7651):498, 2017.

[11] Cristobal Girardi, Josephine Greve, Marc Lamshöft, Ingo Fetzer, Anja Miltner, Andreas Schäffer, and Matthias Kästner. Biodegradation of ciprofloxacin in water and soil and its effects on the microbial communities. *Journal of hazardous materials*, 198:22–30, 2011.

[12] Travis J. Wiles, Elena S. Wall, Brandon H. Schlomann, Edouard A. Hay, Raghuveer Parthasarathy, and Karen Guillemin. Modernized tools for streamlined genetic manipulation and comparative study of wild and diverse proteobacterial lineages. *mBio*, 9(5):e01877–18, 2018.

[13] Kaouther Ben-Amor, Hans Heilig, Hauke Smidt, Elaine E Vaughan, Tjakko Abee, and Willem M de Vos. Genetic diversity of viable, injured, and dead fecal bacteria assessed by fluorescence-activated cell sorting and 16s rrna gene analysis. *Applied and environmental microbiology*, 71(8):4679–4689, 2005.

[14] J. Ganz, R. P. Baker, M. K. Hamilton, E. Melancon, P. Diba, J. S. Eisen, and R. Parthasarathy. Image velocimetry and spectral analysis enable quantitative characterization of larval zebrafish gut motility. *Neurogastroenterology & Motility*, 30(9):e13351, 2018.

[15] Catherine D Robinson, Helena S Klein, Kyleah D Murphy, Raghuveer Parthasarathy, Karen Guillemin, and Brendan JM Bohannan. Experimental bacterial adaptation to the zebrafish gut reveals a primary role for immigration. *PLoS biology*, 16(12):e2006893, 2018.

[16] Pavel L Krapivsky, Sidney Redner, and Eli Ben-Naim. *A kinetic view of statistical physics*. Cambridge University Press, 2010.

[17] Carolina Tropini, Kristen A Earle, Kerwyn Casey Huang, and Justin L Sonnenburg. The gut microbiome: connecting spatial organization to function. *Cell host & microbe*, 21(4):433–442, 2017.

[18] Yuan Gao and Hongzhe Li. Quantifying and comparing bacterial growth dynamics in multiple metagenomic samples. *Nature methods*, 15(12):1041, 2018.

[19] Markus Arnoldini, Jonas Cremer, and Terence Hwa. Bacterial growth, flow, and mixing shape human gut microbiota density and composition. *Gut Microbes*, 9(6):559–566, 2018. PMID: 29533125.

[20] M. Westerfield. The Zebrafish Book. A Guide for the Laboratory Use of Zebrafish (Danio rerio), 5th Edition. *University of Oregon Press, Eugene (Book)*, 2007.

[21] E. Melancon, S. Gomez De La Torre Canny, S. Sichel, M. Kelly, T. J. Wiles, J. F. Rawls, J. S. Eisen, and K. Guillemin. Best practices for germ-free derivation and gnotobiotic zebrafish husbandry. *Methods in Cell Biology*, 138:61–100, 2017.

[22] W. Zac Stephens, Adam R. Burns, Keaton Stagaman, Sandi Wong, John F. Rawls, Karen Guillemin, and Brendan J.M. Bohannan. The composition of the zebrafish intestinal microbial community varies across development. *ISME Journal*, 10:644–654, 2016.

[23] Kathryn Milligan-Myhre, Jeremy R Charette, Ryan T Phennicie, W Zac Stephens, John F Rawls, Karen Guillemin, and Carol H Kim. Study of host–microbe interactions in zebrafish. In *Methods in cell biology*, volume 105, pages 87–116. Elsevier, 2011.

[24] Matthew Jemielita, Michael J Taormina, Adam R Burns, Jennifer S Hampton, Annah S Rolig, Karen Guillemin, and Raghuveer Parthasarathy. Spatial and temporal features of the growth of a bacterial\nspecies colonizing the zebrafish gut. *MBio*, 5(6):1–8, 2014.

[25] Y. Boykov and V. Kolmogorov. An experimental comparison of min-cut/max- flow algorithms for energy minimization in vision. *IEEE Transactions on Pattern Analysis and Machine Intelligence*, 26(9):1124–1137, 2004.

[26] PL Krapivsky and S Redner. Transitional aggregation kinetics in dry and damp environments. *Physical Review E*, 54(4):3553, 1996.

[27] Daniel T Gillespie. Exact stochastic simulation of coupled chemical reactions. *The journal of physical chemistry*, 81(25):2340–2361, 1977.

Supplementary Figure 1 caption

Additional Vibrio data A: Representative masks of fluorescence microscopy images of in vitro viability staining. Top row, untreated, bottom row, 10 ng/mL ciprofloxacin-treated cells (6 hour treatment). SYTO9, shown in green (left panel), indicates intact cells, propridium iodine (PI), shown in magenta (middle panel), indicates dead cells. Double positive cells indicate damaged but viable cells [13], shown in white in the merged, right panel. Scale bar = 100 μm. B: Quantification of in vitro viability staining by fraction of cells corresponding to each case. Mean and standard deviation across 2 replicates shown. C: Representative fluorescence microscopy images of the SOS response in untreated (top row) and 10 ng/mL ciprofloxacin treated (bottom) cells. Constitutive dTom expression is shown in magenta (left), *recN*-linked GFP expression in green (middle), merged images shown in right panel. Scale bar = 50 μm. D: Quantification of SOS response in fraction of SOS+ cells (Methods), mean and standard deviations shown, $n > 4$ per treatment. unt = untreated, cip = 10 ng/mL ciprofloxacin, mmc = 400 ng/mL mitomycin C, amp = 10 μg/mL ampicillin. E: Timeline of in vivo antibiotic treatment. F: In vivo abundances of untreated and 10 ng/mL ciprofloxacin-treated cohorts by day. Each small circle corresponds to a single host, black lines indicate medians and quartiles.

Supplementary Figure 2 caption

Additional Enterobacter data A: Representative fluorescence microscopy images of in vitro viability staining. Top row, untreated, bottom row, 25 ng/mL ciprofloxacin-treated cells (6 hour treatment). SYTO9, shown in green (left panel), indicates intact cells, propridium iodine (PI), shown in magenta (middle panel), indicates dead cells. Double positive cells indicate damaged but viable cells [13], shown in white in the merged, right panel. Scale bar = 100 μm. B: Quantification of in vitro viability staining by fraction of cells corresponding to each case. Mean and standard deviation across 2 replicates shown. C: Timeline of in vivo antibiotic treatment. D: In vivo abundances of untreated and 25 ng/mL ciprofloxacin-treated cohorts by day. Each small circle corresponds to a single host, black lines indicate medians and quartiles. E: Maximum intensity projection of untreated *Enterobacter* population showing an example of a population containing a single large cluster and several single cells. Scale bar = 200 μm.

Supplementary Figure 3 caption

Additional model details A-B: Simulated heatmap of mean (A) and standard deviation (B) of $\log_{10}(\text{abundance} + 1)$ for varying values of aggregation and fragmentation rates. Both mean and standard deviation depend primarily on the ratio of fragmentation to aggregation

rates, rather than on each rate independently. Dashed magenta line in (A) represents $\alpha = \beta$. Parameters: $r = 0.27$ hr^{-1}, $\lambda = 0.11$ hr^{-1}, $K = 10^5$, simulation time = 64 hours, number of trials decreased logarithmically with β from 1000 to 10. Units of α and β are hr^{-1}. C: Heatmap of χ^2 for untreated Enterobacter fit to 7 dpf abundances (Methods). Parameters: $r = 0.27$ hr^{-1}, $\lambda = 0.11$ hr^{-1}, $\alpha = 0.1$ hr^{-1}, simulation time = 64 hours, number of trials decreased logarithmically with β from 1000 to 10. D: χ^2 for fit to 6 dpf ciprofloxacin-treated Enterobacter abundances as a function of the scaling parameter ϵ, which scales the growth and fragmentation rates simultaneously according to $r \to \epsilon r$ and $\beta \to \epsilon\beta$. A clear minimum is seen at $\epsilon = 0.1$. Parameters: $r = 0.27$ hr^{-1}, $\lambda = 0.11$ hr^{-1}, $\alpha = 0.1$ hr^{-1}, $\beta = 10^{1.5}$ hr^{-1}, simulation time = 64 hours, number of trials decreased logarithmically with β from 1000 to 10. E: 3D phase diagram of $\log_{10}$(abundance+1) with axes fragmentation/aggregation (β/α), growth rate (r), and expulsion rate (λ). Blue surface represents $\log_{10}(\text{abundance} + 1) = 0.5 \pm 0.5$, yellow surface represents $\log_{10}(\text{abundance} + 1) = 5.5 \pm 0.5$. Parameters: $\alpha = 0.1$ hr^{-1}, simulation time = 64 hours, number of trials decreased logarithmically with β from 1000 to 10. Units of α and β are hr^{-1}. F: Slices through the 3D phase digram in (E) for different values of λ.

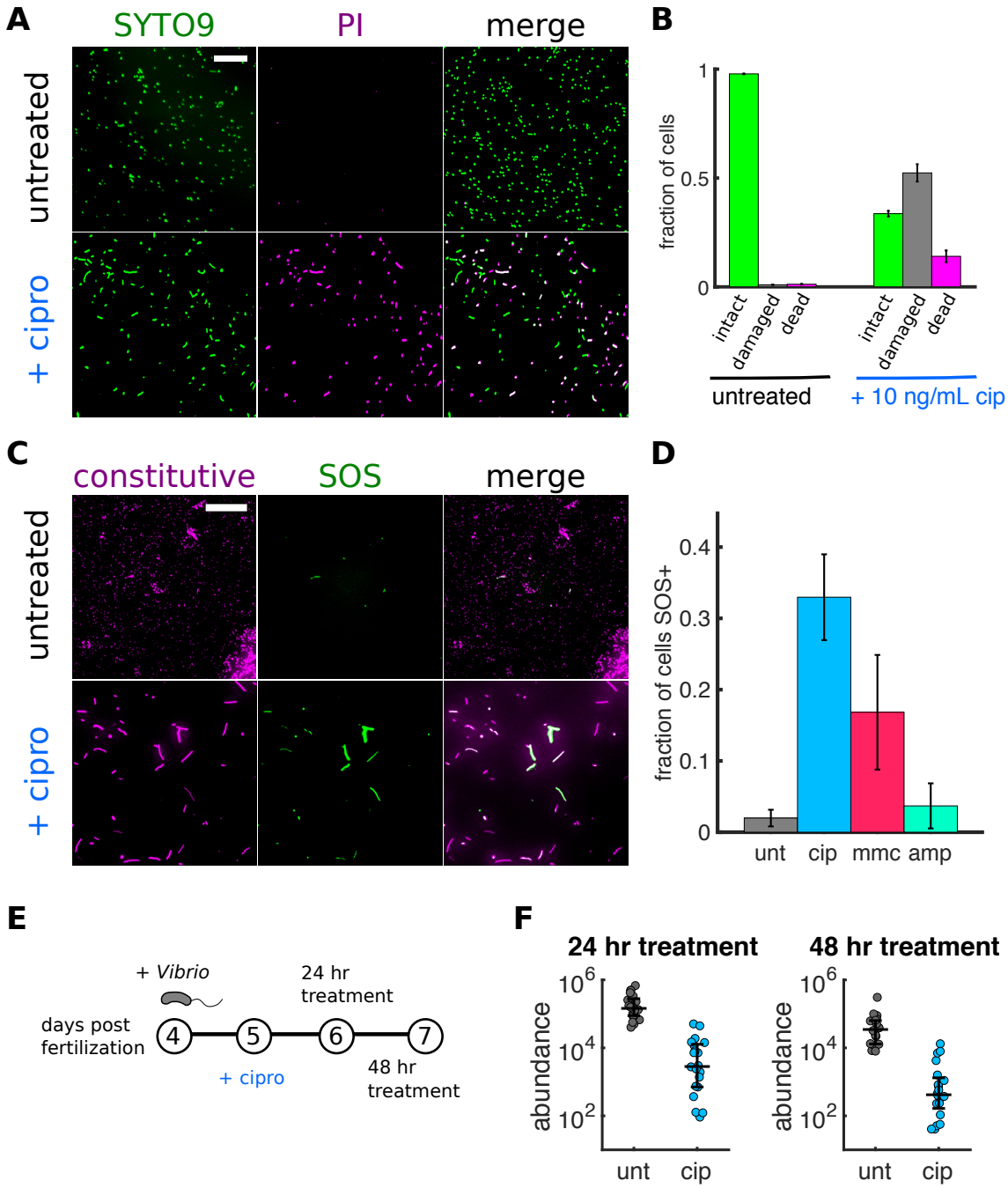
A
SYTO9
PI
merge
untreated
+ cipro
B
fraction of cells
1
0.5
0
intact
damaged
dead
intact
damaged
dead
untreated
+ 10 ng/mL cip
C
constitutive
SOS
merge
untreated
+ cipro
D
fraction of cells SOS+
0.4
0.3
0.2
0.1
0
unt
cip
mmc
amp
E
+ Vibrio
24 hr
treatment
days post
fertilization
4
5
6
7
+ cipro
48 hr
treatment
F
24 hr treatment
48 hr treatment
abundance
10^6
10^4
10^2
unt
cip

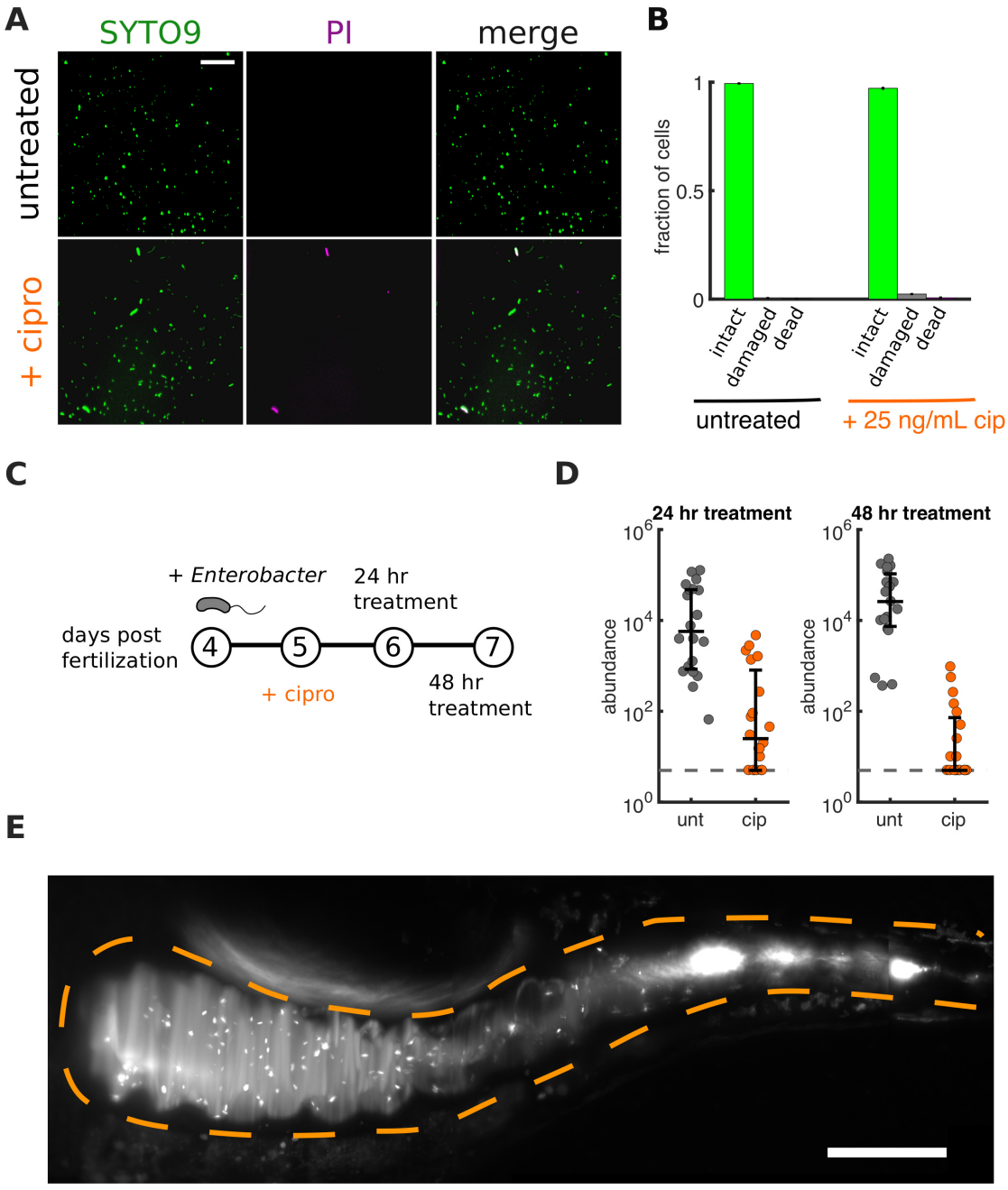
A
SYTO9
PI
merge
untreated
+ cipro
B
fraction of cells
1
0.5
0
intact
damaged
dead
intact
damaged
dead
untreated
+ 25 ng/mL cip
C
+ Enterobacter
24 hr
treatment
days post
fertilization
4
5
6
7
+ cipro
48 hr
treatment
D
24 hr treatment
48 hr treatment
abundance
10^6
10^4
10^2
10^0
unt
cip
E

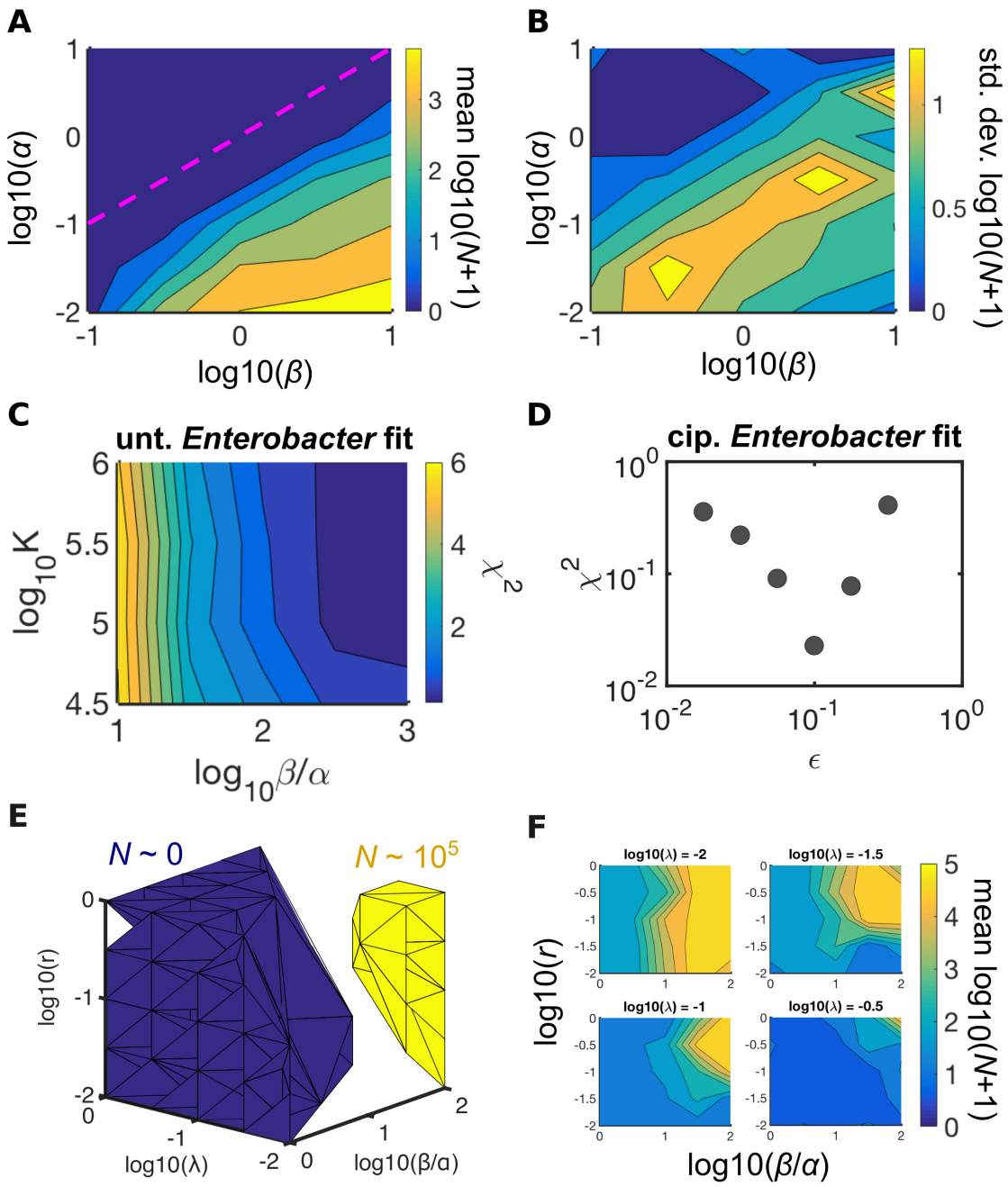
A
log10(α)
log10(β)
mean log10(N+1)
B
log10(α)
log10(β)
std. dev. log10(N+1)
C
unt. Enterobacter fit
log10K
log10β/α
χ2
D
cip. Enterobacter fit
χ2
ϵ
E
N ~ 0
N ~ 10^5
log10(r)
log10(λ)
log10(β/α)
F
log10(λ) = -2
log10(λ) = -1.5
log10(λ) = -1
log10(λ) = -0.5
log10(r)
log10(β/α)
mean log10(N+1)

Supplemental Movie captions

Supplemental Movie 1

Light sheet fluorescence microscopy movie of untreated *Vibrio* swimming in a 6 dpf zebrafish gut. The density of cells is highest on the left (anterior), where single cells cannot be resolved and the population appears as a single bright region (see also Figure 1C). On the right (posterior), single cells are more easily resolved and are seen swimming in and out of the intestinal folds. Each frame is a single optical plane. Scale bar = 50 μm.

Supplemental Movie 2

Animated z-stack of light sheet fluorescence microscopy images of untreated *Enterobacter* in a 6 dpf zebrafish gut. Bacterial clusters (bright white puncta) of diverse sizes are evident, from single cells up to a single cluster containing thousands of cells that appears at a z depth of $\sim$ 70 μm. Hazy reflection of light off of the fish's swim bladder can be seen outside the intestinal boundary in the upper right section of the images. Scale bar = 50 μm.

Supplemental Movie 3

Fluorescence microscopy movie of untreated *Vibrio* swimming between a glass slide and a coverslip (Methods). Scale bar = 10 μm.

Supplemental Movie 4

Fluorescence microscopy movie of *Vibrio* treated with 10 ng/mL ciprofloxacin swimming between a glass slide and a coverslip (Methods). Cells have undergone filamentation. Scale bar = 10 μm.

Supplemental Movie 5

Time-lapse light sheet fluorescence microscopy movie of an established *Vibrio* population responding to 10 ng/mL ciprofloxacin. Each frame is a maximum intensity projection of the full 3D intestinal volume. Time between frames is 20 min. Initially, the population consists of a dense collection of individual, motile cells (Supplemental Movie 1, Figure 1C). Antibiotics are added after the second frame of the movie. Following motility loss, cells leave the swarm and are compacted into aggregates, which are subject to strong transport down

the intestine length and are eventually expelled. The processes of aggregation and transport are driven primarily by rhythmic intestinal contractions that are not captured by our 20 min intervals. Scale bar = 200 μm.

Supplemental Movie 6

Light sheet fluorescence microscopy movies of *Vibrio* in fish treated with 10 ng/mL ciprofloxacin. Left panel movie shows constitutive dTom expression. Right panel movie was taken immediately after the left panel movie and shows a GFP reporter of the SOS response (Methods), which is expressed in cells strongly affected by ciprofloxacin (Supplementary Figure 1C,D). GFP-positive cells swim slowly or are aggregated. Each frame is a single optical plane. Scale bar = 25 μm.

Supplemental Movie 7

Time-lapse light sheet fluorescence microscopy movie of an untreated *Enterobacter* population showing an example of the expulsion process. Each frame is a maximum intensity projection of the full 3D intestinal volume. Time between frames is 10 min. The population is initially comprised of many small bacterial clusters and a single large cluster. Over time, small clusters are incorporated into the large one and the mass is transported down the length of the gut and expelled. The transport process is driven by rhythmic intestinal contractions that occur between frames and are not captured by our 10 min intervals. Images are log-transformed. Scale bar = 200 μm.

Supplemental Movie 8

Time-lapse light sheet fluorescence microscopy movie of an untreated *Enterobacter* population showing an example of the aggregation process. Each frame is a maximum intensity projection of the full 3D intestinal volume. Time between frames is 10 min. A collection of initially disconnected bacterial clusters on the left (anterior) side of the field of view gradually combine into a single cluster. The aggregation process is driven by rhythmic intestinal contractions that occur between frames and are not captured by our 10 min intervals. Images are log-transformed. Scale bar = 200 μm.

Supplemental Movie 9

Time-lapse light sheet fluorescence microscopy movie of an untreated *Enterobacter* population showing examples of the growth and fragmentation processes. Each frame is a maximum

intensity projection of the full 3D intestinal volume. Time between frames is 20 min. The movie begins 8 hours after the initial exposure to *Enterobacter*, by which time a small founding population has been established. Over time, the aggregates grow in size as cells divide, and new single cells also appear in the vicinity of the aggregates, likely due to fragmentation. Individual cell divisions from planktonic cells are also visible. Images are log-transformed. Scale bar = 200 μm.